NANO LETTERS

LETTER

pubs.acs.org/NanoLett

Raman Signature of Graphene Superlattices

Victor Carozo,[†,‡] Clara M. Almeida,[‡] Erlon H. M. Ferreira,[‡] Luiz Gustavo Cançado,[§] Carlos Alberto Achete,[†,‡] and Ado Jorio*[,§]

[†]Departamento de Engenharia Metalúrgica e de Materiais, Universidade Federal do Rio de Janeiro, Rio de Janeiro RJ, 21941-972, Brazil

[‡]Divisão de Metrologia de Materiais, Instituto Nacional de Metrologia, Normalização e Qualidade Industrial (INMETRO), Duque de Caxias RJ 25250-020, Brazil

[§]Departamento de Física, Universidade Federal de Minas Gerais, Belo Horizonte MG 30123-970, Brazil

ABSTRACT:

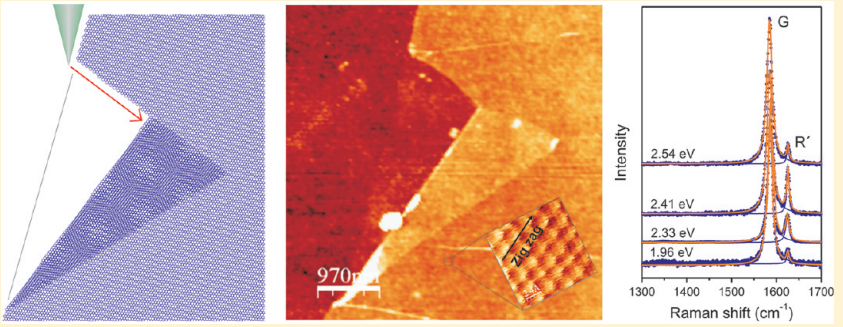

When two identical two-dimensional periodic structures are superposed, a mismatch rotation angle between the structures generates a superlattice. This effect is commonly observed in graphite, where the rotation between graphene layers generates Moiré patterns in scanning tunneling microscopy images. Here, a study of intravalley and intervalley double-resonance Raman processes mediated by static potentials in rotationally stacked bilayer graphene is presented. The peak properties depend on the mismatch rotation angle and can be used as an optical signature for superlattices in bilayer graphene. An atomic force microscopy system is used to produce and identify specific rotationally stacked bilayer graphenes that demonstrate the validity of our model.

KEYWORDS: Graphene, superlattice, Raman spectroscopy, double-resonance Raman, lattice resolution AFM, Moiré pattern

Graphene is a honeycomb lattice made of carbon atoms at the hexagon vertices, with the unit cell composed of two unequivalent carbons, usually named A and B.[1] When two graphenes are placed on top of each other, they can form the Moiré pattern, a superlattice structure generated by a mismatch angle between the top and bottom layer[2] that can be observed in scanning tunneling microscopy images.[3,4] Twisted graphene layers occur naturally at the surface of crystalline graphite[5] and in graphene systems grown by CVD.[6] The mechanical exfoliation method, broadly used to produce graphene systems, can also generate such structures accidentally,[7] and other techniques, such as washing exfoliated graphene with a water flux, can been applied[8] to increase the yield of graphene structures folded into themselves. Interestingly, under special conditions these superlattices can generate electronic flat bands close to the Fermi energy,[9,10] and low energy van Hove singularities in the density of electronic states.[11]

The superlattice generated by a rotationally stacked bilayer graphene is expected to be decorated with a static potential originated from the interaction between the two layers. This potential carries the periodicity of the superlattice and might be able to transfer momentum to photoexcited electrons. In a recent paper, Gupta et al.[7] proposed that this mechanism is responsible for the achievement of momentum conservation in double-resonance Raman processes involving phonons with non-null wavevectors, giving rise to sharp and nondispersive peaks observed around 1400 cm^{-1}. Raman spectroscopy is indeed a very powerful tool broadly used for studying and characterizing sp^2 carbons.[12] The G band near 1584 cm^{-1} is the single first-order Raman allowed peak in graphene, fulfilling momentum conservation, which dictates the scattered phonon should carry no momentum. The Raman spectra of graphene lattices with defects that break the translational symmetry present two disorder-induced features called D and D′ bands.[13−16] The frequency of these two bands depend on the excitation laser energy (E_L), occurring at ∼1350 and ∼1620 cm^{-1}, respectively, for E_L = 2.41 eV. The D and D′ bands are originated from intervalley and intravalley double-resonance Raman scattering mechanisms, respectively.[17,18]

Here we develop a model for the double-resonance Raman processes mediated by the static potentials in rotationally stacked bilayer graphene and predict the presence of Raman bands originated from intravalley and intervalley processes. The resonant excitation laser energy, the frequency, and the strength of

Received: April 24, 2011
Revised: October 5, 2011
Published: October 06, 2011

these bands depend on the rotation angle θ, and the predicted effect can be used to identify the formation of graphene superlattices. To prove our model, a method to produce such structures by means of atomic force microscopy (AFM) is introduced. The Raman spectra of the fabricated superlattices present nondispersive new peaks whose frequency values (Raman shift) and resonance energies are consistent with our model.

Figure 1a shows a rotationally stacked bilayer graphene, with the red layer sitting on top of the blue layer. The top and bottom layers are rotated from each other by a generic angle θ, generating a periodic Moiré pattern. Figure 1b shows this structure in the reciprocal space. $\mathbf{b}_1$ and $\mathbf{b}_2$ are the reciprocal vectors of the bottom layer (blue layer in Figure 1a). These two reciprocal vectors are given as $\mathbf{b}_1 = (2\pi/a)[(\sqrt{3}/3)\hat{\mathbf{k}}_x + \hat{\mathbf{k}}_y]$, and $\mathbf{b}_2 = (2\pi/a)[-(\sqrt{3}/3)\hat{\mathbf{k}}_x + \hat{\mathbf{k}}_y]$, where $a = 2.46$ nm is the lattice parameter of graphene, and $\hat{\mathbf{k}}_x$ and $\hat{\mathbf{k}}_y$ are the unit wavevectors (defined in Figure 1b). $\mathbf{b}_1'$ and $\mathbf{b}_2'$ (see Figure 1b) are the reciprocal vectors relative to the top layer (red layer in Figure 1a), which can be obtained from the direct product between the rotation matrix $\hat{R}(\theta)$ and the wavevectors $\mathbf{b}_1$ and $\mathbf{b}_2$, respectively, giving

$$\mathbf{b}_1'(\theta) = \frac{2\pi}{\sqrt{3}a}[(\cos\theta - \sqrt{3}\sin\theta)\hat{\mathbf{k}}_x + (\sqrt{3}\cos\theta + \sin\theta)\hat{\mathbf{k}}_y] \quad (1)$$

$$\mathbf{b}_2'(\theta) = \frac{2\pi}{\sqrt{3}a}[(-\cos\theta - \sqrt{3}\sin\theta)\hat{\mathbf{k}}_x + (\sqrt{3}\cos\theta - \sin\theta)\hat{\mathbf{k}}_y] \quad (2)$$

As shown in Figure 1a, the mismatch between the two layers gives rise to a periodic superlattice, whose reciprocal rotational vectors $\mathbf{q}_1$ and $\mathbf{q}_2$ can be evaluated by taking the difference between the reciprocal vectors of the two lattices.[19] In terms of the unit vectors $\hat{\mathbf{k}}_x$ and $\hat{\mathbf{k}}_y$, these two reciprocal vectors are given by $\mathbf{q}_1 = \mathbf{b}'_1 - \mathbf{b}_1$ and $\mathbf{q}_2 = \mathbf{b}'_2 - \mathbf{b}_2$, and the result is

$$\mathbf{q}_1(\theta) = \frac{2\pi}{\sqrt{3}a}\{[-(1-\cos\theta) - \sqrt{3}\sin\theta]\hat{\mathbf{k}}_x + [-\sqrt{3}(1-\cos\theta) + \sin\theta]\hat{\mathbf{k}}_y\} \quad (3)$$

$$\mathbf{q}_2(\theta) = \frac{2\pi}{\sqrt{3}a}\{[(1-\cos\theta) - \sqrt{3}\sin\theta]\hat{\mathbf{k}}_x + [-\sqrt{3}(1-\cos\theta) - \sin\theta]\hat{\mathbf{k}}_y\} \quad (4)$$

The absolute value of the rotational wavevectors given in eqs 3 and 4 is:

$$q(\theta) = \frac{8\pi}{\sqrt{3}a}\sin\left(\frac{\theta}{2}\right) \quad (5)$$

It should be noticed that the hexagonal symmetry of the graphene lattice restricts our analysis for $0 \le \theta \le 30°$.

The direct vectors $\mathbf{r}_1$ and $\mathbf{r}_2$ defining the supercell can be obtained from the dot product $\mathbf{r}_i \cdot \mathbf{q}_j = 2\pi\delta_{ij}$, where $\{i,j\} = \{1,2\}$, and δ_{ij} is a Kronecker delta. The result is

$$\mathbf{r}_1(\theta) = -\frac{a}{4}\left[\sqrt{3} + \cot g\left(\frac{\theta}{2}\right)\right]\hat{\mathbf{x}} - \frac{a}{4}\left[1 - \sqrt{3}\cot g\left(\frac{\theta}{2}\right)\right]\hat{\mathbf{y}} \quad (6)$$

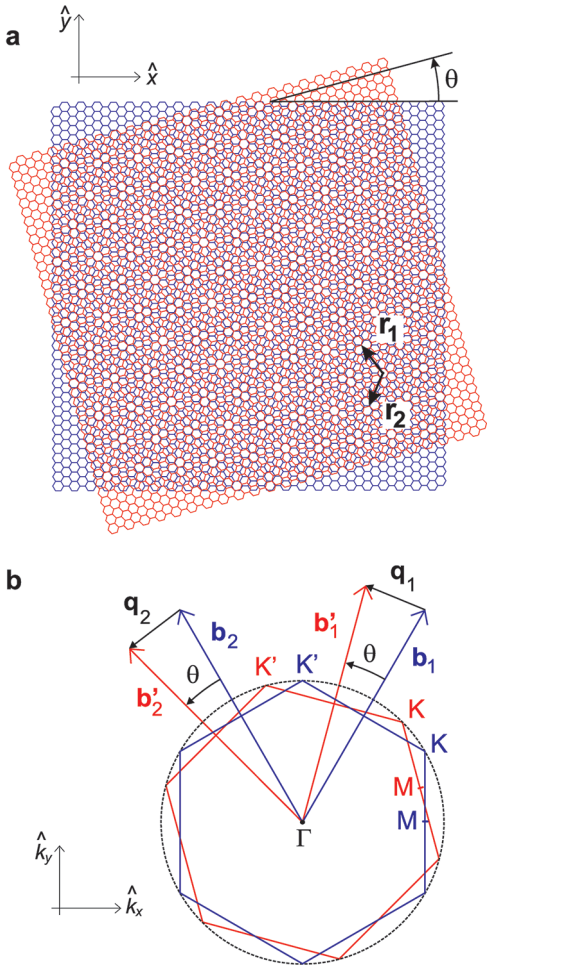

Figure 1. (a) Schematics of a rotationally stacked bilayer graphene with the red layer sitting on the top of the blue layer. The top and bottom layers are rotated from each other by a generic angle θ, generating a periodic Moiré pattern. $\mathbf{r}_1$ and $\mathbf{r}_2$ are the direct vectors defining the supercell, and $\hat{\mathbf{x}}$ and $\hat{\mathbf{y}}$ are the direct unit vectors. (b) The 1st Brillouin zones of the stacked layers shown in panel (a). $\mathbf{b}_1$ and $\mathbf{b}_2$ are the reciprocal vectors of the bottom layer [blue layer in part (a)]. b'_1 and b'_2 are the reciprocal vectors relative to the top layer [red layer in part (a)]. $\hat{\mathbf{k}}_x$ and $\hat{\mathbf{k}}_y$ are the unit wavevectors.

and

$$\mathbf{r}_2(\theta) = \frac{a}{4}\left[\sqrt{3} - \cot g\left(\frac{\theta}{2}\right)\right]\hat{\mathbf{x}} - \frac{a}{4}\left[1 + \sqrt{3}\cot g\left(\frac{\theta}{2}\right)\right]\hat{\mathbf{y}} \quad (7)$$

where $\hat{\mathbf{x}}$ and $\hat{\mathbf{y}}$ are the direct unit vectors. Figure 1a shows the vectors $\mathbf{r}_1$ and $\mathbf{r}_2$ calculated for that specific rotation angle θ. The modulus of the direct vectors, $r_1 = r_2 = a/[2\sin(\theta/2)]$, determines the periodicity of the supercell.[5,19]

Figure 2a shows the Brillouin zones of the top and bottom graphene layers rotated from each other by a small angle θ. Figure 2b shows the schematics of an intravalley double-resonance process involving elastic electron scattering by the static potential. The process starts with the absorption of a photon with energy E_L and wavevector $\mathbf{k}_0$, generating an electron−hole pair with wavevector $\mathbf{k}_{intra}$ measured from the K point. The static potential is able to transfer momentum with the rotational wavevector $\mathbf{q}$ [see eqs 3 to 5], and the electron is elastically scattered to

dx.doi.org/10.1021/nl201370m |Nano Lett. 2011, 11, 4527–4534

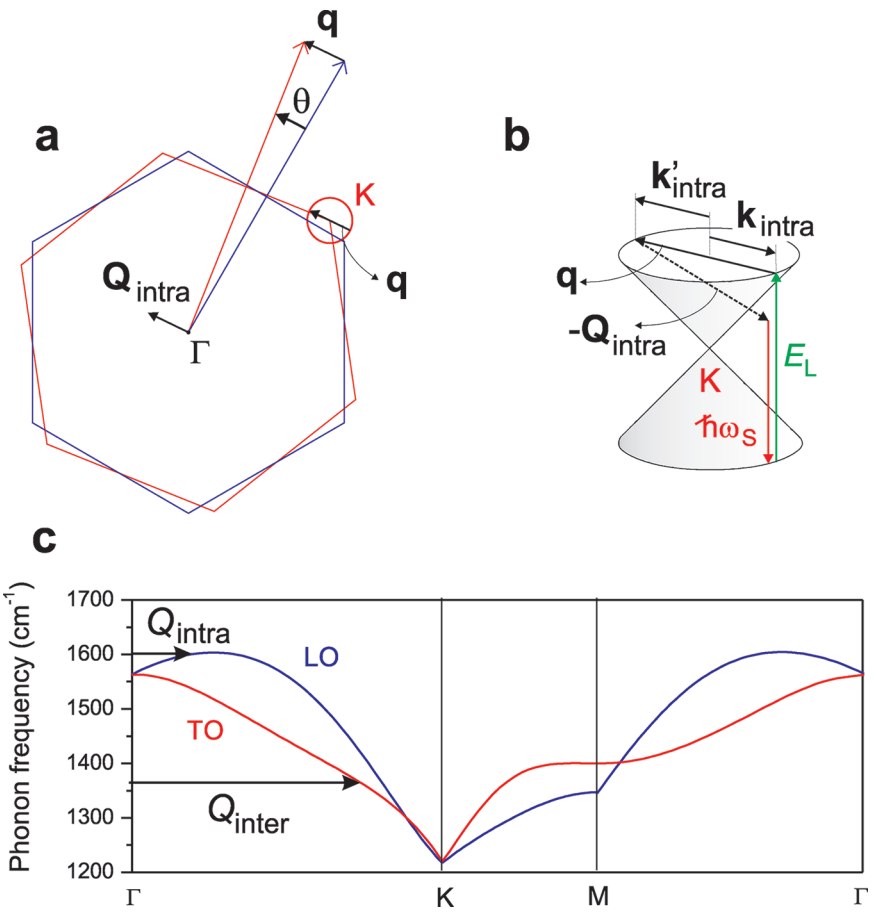

Figure 2. (a) Brillouin zones of the top and bottom graphene layers rotated from each other by a small angle θ. (b) Schematics of an intravalley double-resonance process involving elastic electron scattering by the static potential. (c) High energy in-plane transversal (TO) and longitudinal (LO) optical phonon branches along high symmetry directions in the 1st Brillouin zone of graphene (taken from ref 20). The electron−phonon coupling is stronger for the LO and TO phonon branches near the Γ and K points, respectively,[20] where we assign $\mathbf{Q}_{intra}$ and $\mathbf{Q}_{inter}$.

another point with wavevector $\mathbf{k}'_{intra} = -\mathbf{k}_{intra}$ belonging to the same equienergy circle with radius k_{intra}. A phonon with wavevector $\mathbf{Q}_{intra}$ is then created in the lattice, and the electron is inelastically scattered back to $\mathbf{k}_{intra}$ (or the hole is inelastically scattered to $-\mathbf{k}_{intra}$). These two events are classified as intravalley processes, since they connect two electronic states belonging to the same Dirac cone. Finally, the electron recombines with the hole and a photon with energy $\hbar\omega_S = E_L - \hbar\omega$ (ω being the phonon frequency) and wavevector $\mathbf{k}_S$ is emitted. This process will give rise to a Raman feature, called here the R′ peak (R stands for "rotation", and the ′ superscript is used to keep consistency with the nomenclature used for D and D′ bands). Notice that momentum conservation is only achieved if $\mathbf{k}_0 + \mathbf{k}_S = \mathbf{q}(\theta) - \mathbf{Q}_{intra}(\theta)$ is satisfied. Since k_0 and k_S are small when compared to the size of the 1st Brillouin zone, this momentum conservation condition can be reduced to $\mathbf{Q}_{intra}(\theta) \simeq \mathbf{q}(\theta)$. Visual inspection of Figure 2b clearly show the validity of the latest expression. According to eq 5, the modulus of $\mathbf{Q}_{intra}$ is given by

$$Q_{intra}(\theta) = \frac{8\pi}{\sqrt{3}a}\sin\left(\frac{\theta}{2}\right) \quad (8)$$

Figure 2c shows the high energy in-plane transversal (TO) and longitudinal (LO) optical phonon branches along high symmetry directions in the 1st Brillouin zone of graphene. The phonon dispersion curves were obtained from ref 20. According to Figure 2a, for small angles ($\theta \lesssim 10°$) the wavevector $\mathbf{Q}_{intra}$ lies near the $\mathbf{\Gamma}$ point in the 1st Brillouin zone of graphene, close to the ΓK direction. Since the electron phonon-coupling is specially strong for the LO phonon branch close to the Γ point,[21] the frequency $\omega_{R'}$ can be assigned to that branch. Notice that for larger angles (larger values of Q_{intra}), the R′ band is unlikely to be observed, since the strength of the electron−phonon matrix element is drastically reduced for the LO phonon branch. Figure 3a shows the plot of the R′ band frequency $[\omega_{R'}(\theta)]$ as a function of θ. The conversion $\omega'_R(Q_{intra}) \rightarrow \omega'_R(\theta)$ was obtained by application of eq 8 on the LO phonon dispersion curve shown in Figure 2c along the ΓK direction (the dispersion is isotropic close to the Γ point).

As depicted in Figure 2b, the wavevector $\mathbf{k}_{intra}$ is half of $\mathbf{q}(\theta)$, and the resonance matching between the incident photon energy and the $\pi^* \rightleftharpoons \pi$ transition occurs for $E_L^{intra} = 2k_{intra}\hbar v_F$, where v_F is the Fermi velocity in graphene ($\sim 10^6$ m/s).[22] Therefore, we can use eq 5 to evaluate the value E_L^{intra} for a resonance R′ scattering process, which gives

$$E_L^{intra}(\theta) = \hbar v_F \frac{8\pi}{\sqrt{3}a}\sin\left(\frac{\theta}{2}\right) \quad (9)$$

Figure 3b shows the plot of E_L^{intra} as a function of θ, according to eq 9.

We now turn our attention to the intervalley process depicted in Figure 4a, which is dominant for $\theta \rightarrow 30°$. In this case, the

dx.doi.org/10.1021/nl201370m |Nano Lett. 2011, 11, 4527–4534

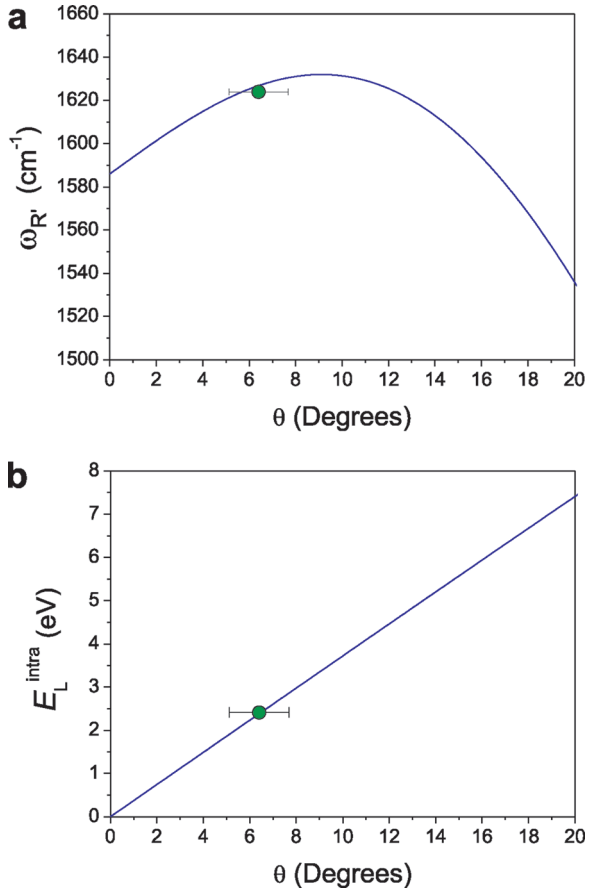

Figure 3. (a) Plot of the frequency of $\omega_{R'}(\theta)$ as a function of θ. $\theta = 0$ corresponds to the LO phonon frequency at the Γ point. (b) Plot of E_L^{intra} as a function of θ. The green circles in panels (a) and (b) are the plot of the experimental data $\omega_{R'} = 1625$ cm^{-1} and $E_L^{intra} = 2.41$, respectively, obtained from the Raman spectra of a twisted graphene bilayer with $\theta \simeq 6°$ [shown in Figure 6]. The error bar indicates the maximum uncertainty in the determination of θ.

rotation wavevector $\mathbf{q}(\theta)$ connects an electronic state with wavevector $\mathbf{k}_{inter}$ (measured from the K point) to an electronic state with wavevector $\mathbf{k}'_{inter}$ (measured from the $\mathbf{K}'$ point), as shown in Figure 4b. From the momentum conservation selection rule, the wavevector of the phonon involved in the Raman process can be related to the rotational wavevector by $\mathbf{Q}_{inter}(\theta) \approx q(\theta)$. As depicted in Figure 4a, this wavevector lies near the K (or K′) point in the first Brillouin zone, an it is more convenient to work with the phonon wavevector $\mathbf{Q}'_{inter}$ (measured from the K point), which can be evaluated as $Q'_{inter}(\theta) = \mathbf{q}(\theta) - \Gamma K$ (see Figure 4b), with modulus

$$Q'_{inter}(\theta) = \frac{4\pi}{3a}\sqrt{7 - 2\sqrt{3}\sin\theta - 6\cos\theta} \qquad (10)$$

Since the electron−phonon coupling near the K point is very strong for the transversal optical (TO) phonon branch, we expect this branch to dominate the intervalley process and to give rise to a Raman feature (called here as R band, without the superscript ′ for consistency with the D and D′ notation). Figure 5a shows the plot of ω_R as a function of θ. The conversion $\omega_R(Q_{inter}) \rightarrow \omega_R(\theta)$ was obtained by applying eq 10 on the TO phonon dispersion curve shown in Figure 2c, along the ΓK direction.

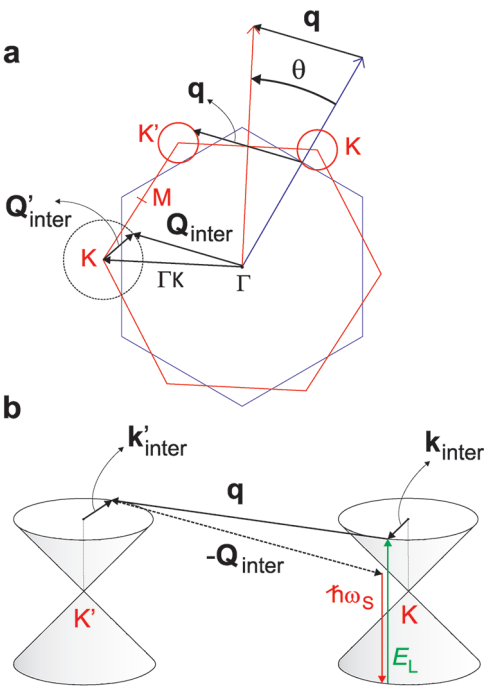

Figure 4. (a) Brillouin zones of the top and bottom graphene layers rotated from each other by a large angle θ. (b) Schematics of an intervalley double-resonance process involving elastic electron scattering by the static potential.

From Figure 4b, it can be seen that the wavevectors $\mathbf{k}_{inter}$ and $\mathbf{k}'_{inter}$ can be obtained as

$$-\mathbf{k}'_{inter}(\theta) = \mathbf{k}_{inter}(\theta) = \left(\frac{1}{2}\right)[\mathbf{q}(\theta) - \mathbf{KK}'] \qquad (11)$$

Considering a linear electronic dispersion near the K and K′ points,[22] we have the resonance condition $E_L^{inter} = 2\hbar v_F k_{inter}$. Application of this resonance condition to eq 11 gives

$$E_L^{inter}(\theta) = \hbar v_F \frac{4\pi}{3a}\sqrt{12\sin^2\left(\frac{\theta}{2}\right) - 2\sqrt{3}\sin\theta + 1} \qquad (12)$$

Figure 5b shows the plot of E_L^{inter} as a function of θ.

It is important to stress that Q_{inter} and Q'_{inter} are uniquely determined by θ [see eqs 8 and 10, respectively]. Therefore, the frequencies of the R′ and R peaks are fixed for a given rotational angle θ, no matter which excitation laser energy is being used in the experiment. This is in contrast with the disorder-induced D′ and D bands, which are dispersive (their frequencies increase with E_L).[13,14] The reason behind this difference is the elastic scattering of the electrons in the double-resonance processes. In the case of the disorder-induced bands, the electron is scattered by potential barriers generated by defects that are usually localized in the real space (e.g., zero-dimensional vacancies[15,16] or one-dimensional edges[23−26]). Zero-dimensional defects are completely delocalized in the reciprocal space, being able to transfer momenta of any magnitude, along any direction. One-dimensional defects (edges) are able to transfer momenta with any magnitude along the direction perpendicular to the edge.[23,25,26] In any case, due to the symmetry of the graphene electronic dispersion in the optical range, the resonance condition for disorder-induced bands will be reached for any excitation laser energy used in the

dx.doi.org/10.1021/nl201370m |Nano Lett. 2011, 11, 4527–4534

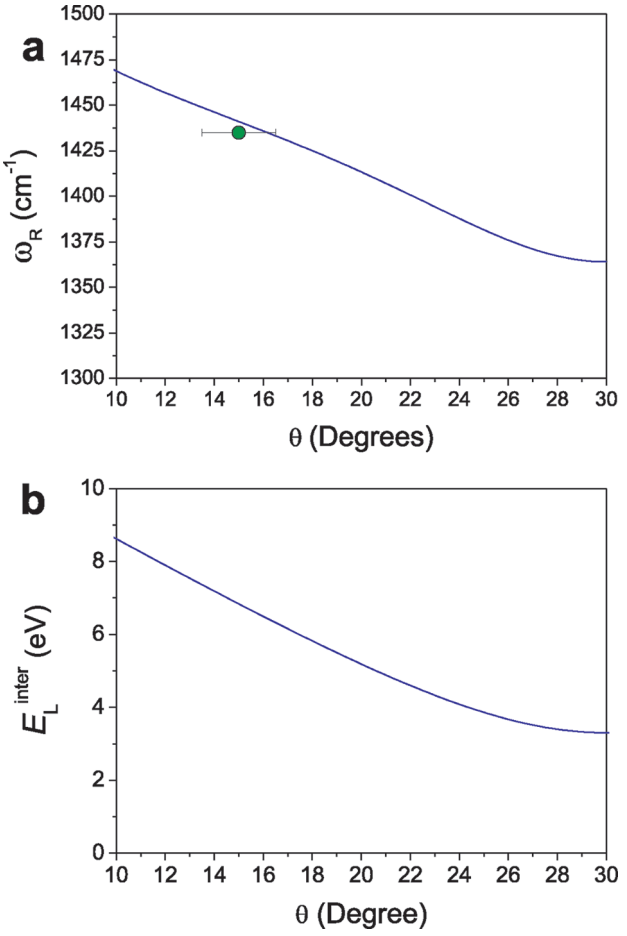

Figure 5. (a) Plot of ω_R as a function of θ. The $\theta = 30°$ corresponds to the TO frequency at the K point. The conversion $\omega_R(Q_{inter}) \rightarrow \omega_R(\theta)$ was obtained by applying eq10 on the TO phonon dispersion curve shown in Figure 2c, along the ΓK direction. (b) Plot of E_L^{inter} as a function of θ. The green circle in panel (a) is the experimental data related to a very weak R feature with unclear resonance behavior obtained from a rotationally stacked bilayer graphene with $\theta \simeq 15°$ (see Figure 7). Notice that the nonresonant character of this feature shown in Figure 7 is due to the relatively high laser energy (~7 eV) necessary for achieving of full resonance condition for $\theta \simeq 15°$.

experiment, since the magnitude of the phonon wavevector can assume whatever value necessary to connect electronic states whose wavevectors are determined by E_L.[27] Since the LO and TO phonon branches are dispersive near the Γ and K points,[21] respectively, the frequencies of the D′ and D bands will also be E_L-dependent.[13,14,17,18] However, this is not the case for the R′ and R bands, whose phonon wavevectors $\mathbf{Q}_{intra}$ and $\mathbf{Q}_{inter}$ are uniquely determined by the rotation wavevector $\mathbf{q}$, which in turn is determined by θ. Finally, the model presented here is based on a double-resonance picture within the extended Brillouin zone. The same results can be obtained with a zone folding procedure.

To prove our model experimentally, we built first a graphene superlattice where the intravalley (R′) process would be likely observed, that is, a rotationally stacked bilayer graphene with a small θ (see Figure 4). Graphene samples were prepared via micromechanical exfoliation of natural graphite (from Nacional de Grafite) onto a substrate composed by n^+-doped Si with a SiO_2 layer (300 nm) on top. Monolayer graphenes were primarily identified using an optical microscope, based on contrast between the flake and the substrate, and then by Raman spectroscopy, based on the shape of the G′ band (~2700 cm^{-1}).[28] Graphene folding was produced by line scanning the sample with a silicon nitride atomic force microscopy (AFM) tip on the contact mode, with resonant frequency of 3.0 kHz and a set point of 1 V. The forces employed by the tip on the sample are capable of cutting and folding the sheet. Atomic force images were obtained in sequence, using an AFM (JPK NanoWizard AFM) operated in air (see Figure 6a). The topography AFM images were acquired in tapping mode using a silicon nitride tip. The measurements of the crystallographic orientation of graphene edge (see inset to Figure 6a) were performed by means of lattice resolution atomic force microscopy in lateral force mode (MultiMode model by Veeco, Santa Barbara, CA). All lateral force images were acquired using a silicon nitride V-shape cantilever with calibrated normal and torsional spring constants of 0.075 ± 0.001 and 68.5 ± 2.57 N/m, respectively. The AFM measurements were carried out in contact mode operated in ambient air. A piezoelectric scanner with 1 μm^2 of maximum scan range was used and the microscope gains were set close to zero. The scanning was performed at 40 Hz in constant height mode.[29]

Raman scattering experiments were performed with two different systems. (i) A Horiba Jobin-Yvon T64000 triple-monochromator equipped with a N_2 cooled charge-coupled-device (CCD) detector in the backscattering configuration with 1800 lines/mm grating, using a 100× objective at room temperature, for the laser energies (wavelengths): He−Ne 1.96 eV (633 nm); argon 2.41 eV (514 nm), 2.54 eV (488 nm) (see Figure 6c). The laser power was always less than 1 mW. The spot size was about 1 μm. (ii) Raman mapping WITEC alpha300 system equipped with an $x-y$ piezostage, using backscattering configuration and a 600 lines/mm grating (see Figure 6d,e). The detected intensity was obtained by means of a CCD. The excitation source is a 2.33 eV diode laser (532 nm) with a laser power below 0.1 mW, and the laser spot size is estimated to be ~350 nm. A 100× objective lens with a 0.95 NA was used. The analysis uses the WITEC Project software.

Figure 6a shows the AFM image of the folded graphene. The crystallographic orientation of the bottom layer was obtained using high-resolution AFM (see inset to Figure 6a). The rotational angle $\theta = (6 \pm 2)°$ was determined from the relative angle between the zigzag orientation and the folding line. Figure 6b shows the schematics of the folding procedure. Notice that a Moiré pattern is generated at the folded region due to the $\theta \sim 6°$ rotation between the layers.

Figure 6c shows the Raman spectra of the rotationally stacked graphene shown in panel a, using four different excitation laser energies: E_L = 1.96, 2.33, 2.41, and 2.54 eV. Besides the first-order allowed G band (~1584 cm^{-1}), a peak centered at ~1625 cm^{-1} is observed. The peak is nondispersive and presents a higher intensity for the spectrum obtained using E_L = 2.41 eV (the spectra are normalized to the G band). Figure 6d shows a Raman image obtained from the same region shown in panel a. The color scale renders the G band intensity. Notice that the G band signal can be detected from the whole graphene piece, and its intensity in the folded region is roughly twice the intensity obtained from the rest of the piece. This is expected, since the G band intensity is almost linearly proportional to the number of layers in few-layer graphene.[30] Figure 6e shows the Raman intensity image of the peak centered at ~1625 cm^{-1}. The image shows that this peak can only be detected when the laser spot is focused on the folded region.

The experimental observations described above are all consistent with a rotational-induced intervalley double-resonance

dx.doi.org/10.1021/nl201370m |Nano Lett. 2011, 11, 4527–4534

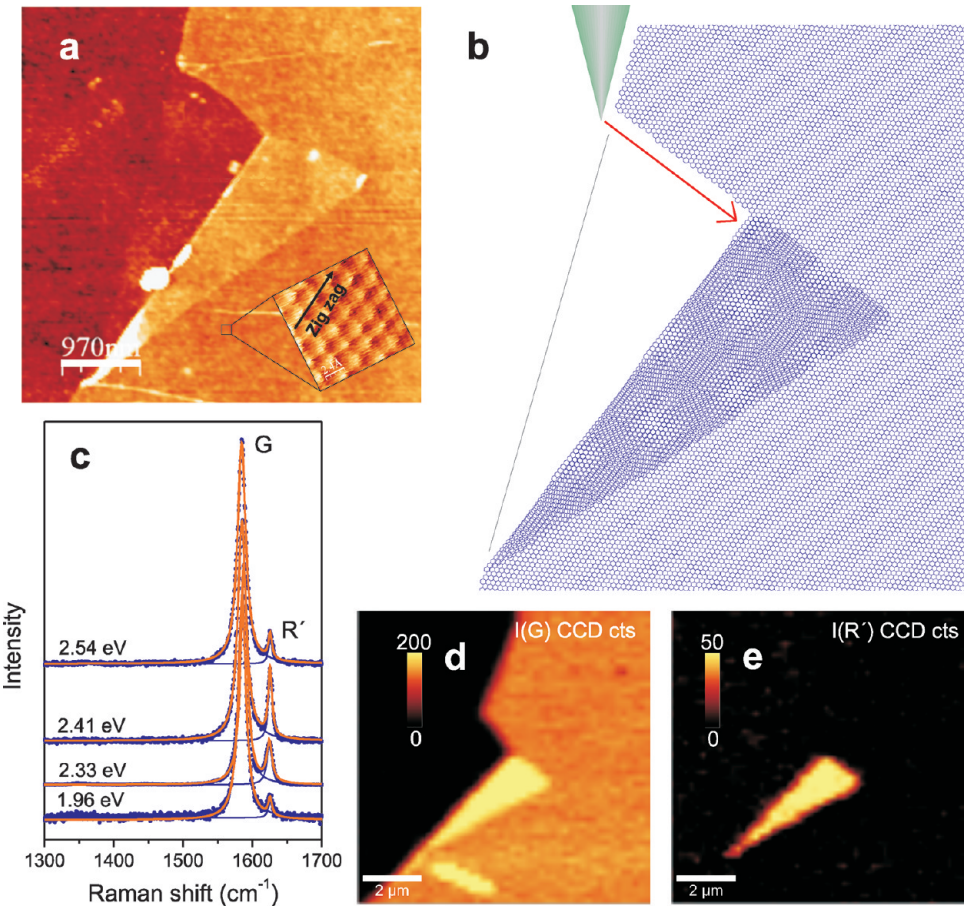

Figure 6. (a) AFM image of a folded graphene. The inset shows a high-resolution AFM image which determines the zigzag crystallographic orientation of the bottom layer. The rotational angle $\theta = (6 \pm 2)°$ was determined as twice the angle between the zigzag orientation and the folding line. (b) Schematics of the folding procedure. Notice that a Moiré pattern is generated at the folded region. (c) Raman spectra of the rotationally stacked graphene shown in panel a, using four different excitation laser energies: E_L = 1.96, 2.33, 2.41, and 2.54 eV. Besides the first-order allowed G band ($\sim$ 1584 cm^{-1}), a peak centered at $\sim$1625 cm^{-1} is observed. The absence of the disorder induced D band ($\sim$ 1350 cm^{-1}) presents evidence that this region has a low defect density. (d) Raman image obtained from the same region shown in panel a. The color scale renders the G band intensity. (e) Raman intensity image of the peak centered at $\sim$1625 cm^{-1}. The image shows that this peak can only be detected when the laser spot is focused on the folded region.

mechanism, as predicted in Figure 3. From $\omega_{R'} = 1625$ cm^{-1}, we can conclude that this is an intravalley R′ peak (see Figure 3a) and the results are in excellent agreement with the predictions of Figure 3a,b (see the agreement between theory lines and the green circles for experimental data). It is important to stress that this peak cannot be assigned as the disorder-induced D′ band. The D′ band has a $\sim$10 cm^{-1}/eV dispersion rate in the visible range[13,14] and it is always much weaker than the D band.[15,16] The absence of the disorder induced D band presents strong evidence that this region has a low defect density.

In sequence, we built a graphene supperlattice with a larger θ, where we expected to observe an R peak originated from intervalley scattering process with frequency below the G band frequency. In this case, from high-resolution AFM we identify $\theta = (15 \pm 2)°$ (see inset to Figure 7a), and observed a new Raman peak at $\omega_R = 1435$ cm^{-1} (see Figure 7b), which can be observed only in the folded region (see Figure 7d). The frequency of this R feature is in good agreement with the theoretical prediction shown in Figure 5a (see agreement between theory line and experimental green circle). The R feature is very weak (about 100 times weaker than the G band) for all laser lines used in the experiment (2.33, 2.41, and 2.54 eV), suggesting that the resonance condition is far away. This is also in agreement with the theoretical curve plotted in Figure 5b that predicts a much higher laser energy ($\sim$7 eV) necessary for achieving full resonance condition for $\theta \simeq 15°$.

In addition, we measured the Raman spectra of six other AFM generated folded structures that presented R or R′ peaks (not shown). Although we were not able to measure high-resolution AFM in all these cases, the observed ω_R and $\omega_{R'}$ are always within the expected frequency range shown in Figures 3 and 5, and therefore their rotational angles θ can be assigned using our theory. We also compared the theory developed here for intervalley processes with the experimental data presented in ref 7. In this work, the authors reported the Raman spectra of rotationally stacked bilayer graphenes, and observed several nondispersive peaks centered at $\sim$1370, $\sim$1385, and $\sim$1395 cm^{-1}. From these frequencies values, we can conclude that all these peaks are originated from intervalley processes (see Figure 5a). The authors also showed Raman spectra of a specific sample obtained using different excitation laser energies, namely E_L = 1.92, 2.41, 2.54, 2.71, and 3.42 eV. The data show a nondispersive peak centered at $\sim$1385 cm^{-1}, whose intensity is strongly enhanced for

dx.doi.org/10.1021/nl201370m |Nano Lett. 2011, 11, 4527–4534

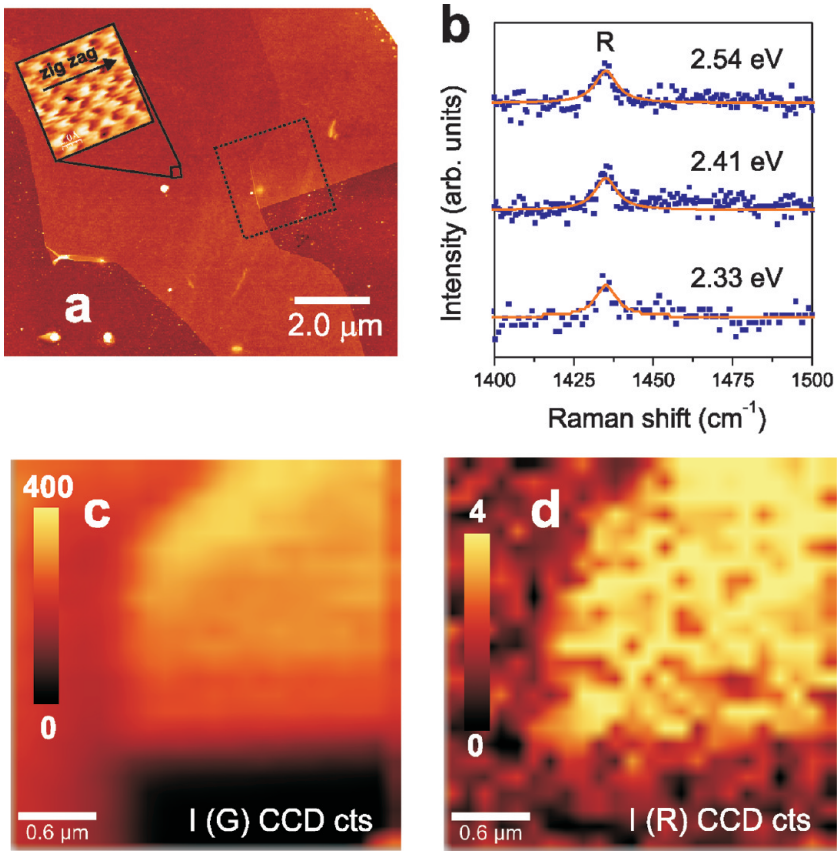

Figure 7. (a) AFM image of a folded graphene. The inset shows a high-resolution AFM image revealing the zigzag crystallographic orientation of the bottom layer. The rotational angle $\theta = (15 \pm 2)°$ was determined as twice the angle between the zigzag orientation and the folding line. (b) Raman spectra of the rotationally stacked graphene shown in panel a, using three different excitation laser energies: $E_L = 2.33$, 2.41, and 2.54 eV. A peak centered at $\sim$1435 cm^{-1} is observed. In all cases (all leaser energies), the intensity is 100 times weaker than the G band. The absence of the disorder induced D band ($\sim$ 1350 cm^{-1}) presents evidence that this region has a low defect density. (c) Raman image obtained from the region highlighted by the dotted square box in panel a. The color scale renders the G band intensity. (d) Raman intensity image of the peak centered at $\sim$1435 cm^{-1} from the same region shown in panel c. The image shows that this peak can only be detected when the laser spot is focused on the folded region.

E_L = 3.42 eV. This result is in good agreement with our calculations shown in Figure 5, where the values $E_L \sim 3.30$ eV and $\omega_R \sim 1370$ cm^{-1} are expected for the R band scattering occurring for $\theta \sim 30°$.

In summary, one can build a graphene superlattice by folding a single layer graphene with an atomic force microscopy (AFM) tip. Identifying the structural formation of superlattices had being, up to now, limited to scanning tunneling microscopy (STM) or scanning tunneling spectroscopy (STS) experiments. Here we showed that Raman spectroscopy can be used as a simpler procedure for identifying the formation of such lattices. Our results prove that a rotationally stacked bilayer graphene is decorated with a static potential, originated from the interaction between the two layers, and this potential is able to transfer momentum to photoexcited electrons, generating a symmetry selective double-resonance Raman scattering process, as first proposed by Gupta et al.[7] The details for the determination of the symmetry of the graphene superlattices via Raman spectroscopy are introduced.

AUTHOR INFORMATION

Corresponding Author

*E-mail: adojorio@fisica.ufmg.br.

ACKNOWLEDGMENT

A.J. acknowledges Mauricio Terrones, Vincent Meunier and B. G. Sumpter for helpful discussions. The authors also acknowledge Benjamin Fragneud for helpful discussions, R. Priolo and Pedro M. Bedê for support on the AFM images. This work was financed by Inmetro and FAPERJ. L.G.C. and A.J. acknowledge support from the Brazilian agencies CNPq and FAPEMIG.

REFERENCES

(1) Wallace, P. R. The Band Theory of Graphite. *Phys. Rev.* **1947**, *71*, 622–634.

(2) Mele, E. J. Commensuration and interlayer coherence in twisted bilayer graphene. *Phys. Rev. B* **2010**, *81*, R161405–R161409.

(3) Tománek, D.; Louie, S. G.; Mamin, H. J.; Abraham, D. W.; Thomson, R. E.; Ganz, E.; Clarke, J. Theory and observation of highly asymmetric atomic structure in scanning-tunneling-microscopy images of graphite. *Phys. Rev. B* **1987**, *35*, 7790–7793.

(4) Cisternas, E.; Flores, M.; Vargas, P. Superstructures in arrays of rotated graphene layers: Electronic structure calculations. *Phys. Rev. B* **2008**, *78*, 125406–125410.

(5) Pong, W. T.; Durkan, C. A review and outlook for an anomaly of scanning tunnelling microscopy (STM): Superlattices on graphite. *J. Phys. D* **2005**, *38*, R329–R355.

(6) N'Diaye, A. T.; Coraux, J.; Plasa, T. N.; Busse, C.; Michely., T. Structure of epitaxial graphene on Ir(111). *New J. Phys.* **2008**, *10*, 043033–043048.

(7) Gupta, A. K.; Tang, Y.; Crespi, V. H.; Eklund, P. C. Non-dispersive Raman D band activated by well-ordered interlayer interactions in rotationally stacked bilayer graphene. *Phys. Rev. B* **2011**, *82*, R241406–R241409.

(8) Poncharal, P.; Ayari, A.; Michel, T.; Sauvajol, J. L. Raman spectra of misoriented bilayer graphene. *Phys. Rev. B* **2008**, *78*, 113407–113410.

(9) Morell, E. S.; Correa, J. D.; Vargas, P.; Pacheco, M.; Barticevic, Z. Flat bands in slightly twisted bilayer graphene: Tight-binding calculations. *Phys. Rev. B* **2010**, *82*, R121407–R121410.

(10) Laissardiére, G. T.; Mayou, D.; Mangaud, L. Localization of Dirac Electrons in Rotated Graphene Bilayers. *Nano Lett.* **2010**, *10*, 804–808.

(11) Li, G.; Luican; Lopes dos Santos, A. J. M. B.; Castro Neto, A. H.; Reina, A.; Kong, J.; Andrei, E. Y. Observation of Von Hove singularities in twisted graphene layers. *Nat. Phys.* **2010**, *6*, 109–113.

(12) Dresselhaus, M. S.; Jorio, A.; Hofmann, M.; Dresselhaus, G.; Saito, R. Perspectives on Carbon Nanotubes and Graphene Raman Spectroscopy. *Nano Lett.* **2010**, *10*, 751–758.

(13) Ferrari, A. C. Raman spectroscopy of graphene and graphite: Disorder, electron-phonon coupling, doping and nonadiabatic effects. *Solid State Commun.* **2007**, *143*, 47–57.

(14) Pimenta, M. A.; Dresselhaus, G.; Dresselhaus, M. S.; Cançado, L. G.; Jorio, A.; Saito, R. Studying disorder in graphite-based systems by Raman spectroscopy. *Phys. Chem. Chem. Phys.* **2007**, *9*, 1276–1291.

(15) Lucchese, M. M.; Stavale, F.; Ferreira, E. H.; Vilani, C.; Moutinho, M. V. O.; Capaz, R. B.; Achete, C. A.; Jorio, A. Quantifying ion-induced defects and Raman relaxation length in graphene. *Carbon* **2010**, *48* (5), 1592–1597.

(16) Cançado, L. G.; Jorio, A.; Martins Ferreira, E. H.; Stavale, F.; Achete, C. A.; Capaz, R. B.; Moutinho, M. V. O.; Lombardo, A.; Kulmala, T. S.; Ferrari, A. C. *Nano Lett.* **2011**, *11* (8), 3190–3196.

(17) Thomsen, C.; Reich, S. Double resonant Raman scattering in graphite. *Phys. Rev. Lett.* **2000**, *85*, 5214–5217.

(18) Saito, R.; Jorio, A.; Souza Filho, A. G.; Dresselhaus, G.; Dresselhaus, M. S.; Pimenta, M. A. Probing phonon dispersion relations of graphite by double resonance Raman scattering. *Phys. Rev. Lett.* **2001**, *88*, 027401–027404.

(19) Miller, D. L.; 1 Kubista, K. D.; Rutter, G. M.; Ruan, M.; de Heer, W. A.; First, P. N.; Stroscio, J. A. Structural analysis of multilayer graphene via atomic Moiré interferometry. *Phys. Rev. B* **2010**, *81*, 125427–125432.

(20) Venezuela, P.; Lazzeri, M.; Mauri, F. Theory of double-resonant Raman spectra in graphene: intensity and line shape of defect-induced and two-phonon bands. *Phys. Rev. B* **2011**, *84*, 035433–035457.

(21) Piscanec, S.; Lazzeri, M.; Mauri, F.; Ferrari, A. C.; Robertson, J. Kohn anomalies and electron-phonon interactions in graphite. *Phys. Rev. Lett.* **2004**, *93*, 185503–185506.

(22) Castro Neto, A. H.; Guinea, F.; Peres, N. M. R.; Novoselov, K. S.; Geim, Geim, A. K. The electronic properties of graphene. *Rev. Mod. Phys.* **2009**, *81*, 109–162.

(23) Cançado, L. G.; Pimenta, M. A.; Neves, B. R. A.; Dantas, M. S. S.; Jorio, A. Influence of the atomic structure on the Raman spectra of graphite edges. *Phys. Rev. Lett.* **2004**, *93*, 247401–247404.

(24) Beams, R.; Cançado, L. G.; Novotny, L. Low-Temperature Raman Study of the Electron Coherence Length near Graphene Edges. *Nano Lett.* **2011**, *11*, 1177–1181.

(25) Casiraghi, C.; Hartschuh, A.; Qian, H.; Piscanec, S.; Georgi, C.; Fasoli, A.; Novoselov, K. S.; Basko, D. M.; Ferrari, A. C. Raman Spectroscopy of Graphene Edges. *Nano Lett.* **2009**, *9*, 1433–1441.

(26) Krauss, B.; Nemes-Incze, P.; Skakalova, V; Biro, L. P.; von Klitzing, K.; Smet, J. H. Raman Scattering at Pure Graphene Zigzag Edges. *Nano Lett.* **2010**, *10*, 4544–4548.

(27) There is a restriction for perfect zigzag edges, which are not able to transfer the required momentum for electrons in intervalley double-rsonance processes. For details, see refs 23, 25, and 26.

(28) Ferrari, A. C.; Meyer, J. C.; Scardaci, V.; Casiraghi, C.; Lazzeri, M.; Mauri, F.; Piscanec, S.; Jiang, D.; Novoselov, K. S.; Roth, S.; Geim, A. K. Raman Spectrum of Graphene and Graphene Layers. *Phys. Rev. Lett.* **2006**, *97*, 187401–187403.

(29) Almeida, C. M., Carozo, V., Prioli, R. Achete, C. A. Easy identification of graphene edges crystallographic orientation by atomic force microscopy. To appear in Journal of Applied Physics, **2011**.

(30) Ni, Z.; Wang, Y.; Yu, T.; Shen, Z. Raman Spectroscopy and Imaging of Graphene. *Nano Res.* **2008**, *1*, 273–291.